Infrared studies of hole-plasmon excitations in heavily-doped *p*-type MBE-grown GaAs:C

W. Songprakob and R. Zallen

Department of Physics, Virginia Tech, Blacksburg, Virginia 24061-0435

W. K. Liu and K. L. Bacher*

Quantum Epitaxial Designs, Inc., Bethlehem, Pennsylvania 18015

(Received 7 September 1999; revised manuscript received 10 April 2000)

Infrared reflectivity measurements (200–5000 cm^{-1}) and transmittance measurements (500–5000 cm^{-1}) have been carried out on heavily-doped GaAs:C films grown by molecular-beam epitaxy. With increasing carbon concentration, a broad reflectivity minimum develops in the 1000–3000 cm^{-1} region and the one-phonon band near 270 cm^{-1} rides on a progressively increasing high-reflectivity background. An effective-plasmon/one-phonon dielectric function with only two free parameters (plasma frequency ω_p and damping constant γ) gives a good description of the main features of both the reflectivity and transmittance spectra. The dependence of ω_p^2 on hole concentration p is linear; at $p = 1.4 \times 10^{20}$ cm^{-3}, ω_p is 2150 cm^{-1}. At each doping, the damping constant γ is large and corresponds to an infrared hole mobility that is about half the Hall mobility. Secondary-ion mass spectroscopy and localized-vibrational-mode measurements indicate that the Hall-derived p is close to the carbon concentration and that the Hall factor is close to unity, so that the Hall mobility provides a good estimate of actual dc mobility. The observed dichotomy between the dc and infrared mobilities is real, not a statistical-averaging artifact. The explanation of the small infrared mobility resides in the influence of intervalence-band absorption on the effective-plasmon damping, which operationally determines that mobility. This is revealed by a comparison of the infrared absorption results to Braunstein's low-p p-GaAs spectra and to a **k·p** calculation extending Kane's theory to our high dopings. For *n*-GaAs, which lacks infrared interband absorption, the dc and infrared mobilities do not differ.

I. INTRODUCTION

Carbon is an attractive dopant for *p*-type GaAs. Recently, a number of growth techniques, including metallo-organic chemical vapor deposition,[1–3] metallo-organic vapor phase epitaxy,[4–7] chemical beam epitaxy,[8] and molecular-beam epitaxy (MBE),[3,9–13] have made it possible to achieve carbon-doped thin-film fabrication with hole concentrations as high as 1.5×10^{21} cm^{-3}.[12] C-doped GaAs has been shown to have advantages over Be-doped and Zn-doped GaAs for applications in devices requiring $p++$ GaAs layers. These advantages include: higher hole mobilities, indicating less compensation;[3,4,6,7,10] preferential incorporation on As sites as substitutional acceptors, resulting in higher electrical activation;[1,3,8,13] and lower diffusivity.[2,9] A notable application of C-doped GaAs (GaAs:C) is its use in the base region of a heterojunction bipolar transistor, where it yields a high current gain.[6,7,10,11] Most studies on GaAs:C in the past ten years were devoted to electrical and structural characterization. A few were conducted to gain fundamental understanding of doping effects and free carriers, using optical experiments: photoluminescence,[14,15] Raman,[16,17] and infrared measurements.[15]

In the present work, we have carried out infrared reflectivity and transmission experiments (covering a broad spectral range from 200 to 5000 cm^{-1}) on MBE GaAs:C films in order to directly observe hole-plasmon excitations as well as their interaction with lattice vibrations. Raman-scattering experiments are usually used to probe such excitations. But for *p*-type GaAs, the higher-frequency (L_+) phonon-plasmon mode cannot be observed in Raman scattering. (At high doping, the L_+ mode frequency lies well above the phonon range and the L_+ mode is essentially plasmonlike.) The non-occurrence of the L_+ in the Raman spectrum of *p*-type GaAs was reported by Olego and Cardona[18] in their extensive studies of GaAs:Zn. The same observation (or, more accurately, nonobservation) has been reported for GaAs:Be,[19] and GaAs:Ge.[20] Most recently, the Raman nonoccurrence of the L_+ has also been reported for GaAs:C.[16,17] Most of these papers attribute the Raman inaccessibility of the L_+ to large damping of the hole plasmon in *p*-type GaAs. In the IR work that we report in this paper, we do indeed confirm the presence of large hole-plasmon damping. It should be noted, however, that there is another important reason for the inability of Raman experiments to discern the L_+ plasmonlike mode in highly doped *p*-type GaAs: competition with strong, Raman-allowed, intervalence-band transitions among the heavy-hole, light-hole, and split-off valence bands.[17,21]

For photon energies well below the band gap, the dispersion of the optical dielectric function in doped GaAs arises from the interactions among photons, phonons, and plasmons. The Drude model provides the simplest approximation for the contribution, to the optical dielectric function, of the free-carrier plasma. It has been successfully applied to *n*-type GaAs,[22–24] in which electrons occupy a single conduction band, using a single plasmon frequency and damping constant. For *p*-type material, the free carriers are holes which populate two different bands, the heavy-hole and light-hole bands, to different extents in *k* space. A complex simulation to treat two plasmas would involve many parameters of doubtful significance. Intervalence-band transitions add another complication. We have chosen to take a minimalist approach and analyze our measurements using the simple

Drude form, involving only two free parameters: the plasma frequency and the damping constant. This effective-plasmon approach adequately accounts for the main features of our experimental results, both in reflectivity and transmittance. The influence of intervalence-band transitions is found in the observed large optical damping, which corresponds to a broad maximum in absorption at high doping and an infrared hole mobility smaller than the dc (Hall) hole mobility. This mobility difference is shown to be real; it is not an artifact of the statistical approximations involved in the estimation of either the Hall or the infrared mobilities.

Experimental techniques are described in Sec. II. Infrared reflectivity results for 12 MBE GaAs:C samples are presented in Sec. III, along with the intensity-matrix transfer-method analysis appropriate for our layer geometry. This section contains our results for the hole-concentration dependence of the plasma frequency and the infrared hole mobility. Section IV presents our infrared transmission results and a comparison of these data to the reflectivity-derived optical dielectric functions of Sec. III. Those effective-plasmon dielectric functions give a good account of the observed absorption data, with a broad, featureless, low-energy absorption maximum appearing at high doping. Calculations based on the **k·p** theory of intervalence-band transitions indicate that such transitions contribute significantly to that broad absorption. The difference between the measured infrared hole mobility and the dc (Hall) hole mobility is discussed in Sec. V. We show that, for our highest dopings, this difference is real and is not a consequence of the standard statistical approximations involved in the determination of either the Hall or infrared mobilities. Instead, we attribute the dc/infrared mobility difference to the additional damping contribution present in the infrared because of intervalence-band optical absorption. Section VI summarizes our main findings.

II. EXPERIMENT

Carbon-doped p-type GaAs films, with hole concentrations ranging from 3.4×10^{18} cm^{-3} to 1.36×10^{20} cm^{-3}, were grown on (100) semi-insulating GaAs substrates by molecular-beam epitaxy, using an EPI GENII MBE reactor. The growth rate was controlled at 2.5 Å /sec, with the substrate kept at the standard GaAs growth temperature of 600 °C. A thin (1000–2500 Å) undoped buffer layer was deposited first; this was found to improve the crystalline quality of the later carbon-doped film. For the carbon-doped layer, a custom-designed C injector was employed with a CBr$_4$ source kept at 0 °C. The thickness of the epitaxial GaAs:C film was varied from 3500 to 7500 Å . Hole concentrations and mobilities were determined by Hall-effect measurements at room temperature, and carbon concentrations for several samples were estimated by secondary-ion-mass spectroscopy (SIMS) and localized vibrational mode spectroscopy (LVM).[25]

The reflectivity and transmittance of 12 GaAs:C MBE films was measured over the wave-number ranges from 200 to 5000 and 500 to 5000 cm^{-1}, respectively, using a Bomem DA3 Fourier-transform spectrometer. Measurements were carried out at room temperature, using an angle of incidence of 11° (with a gold mirror as a reference) for reflectivity and using normal incidence for transmittance. A globar source, a
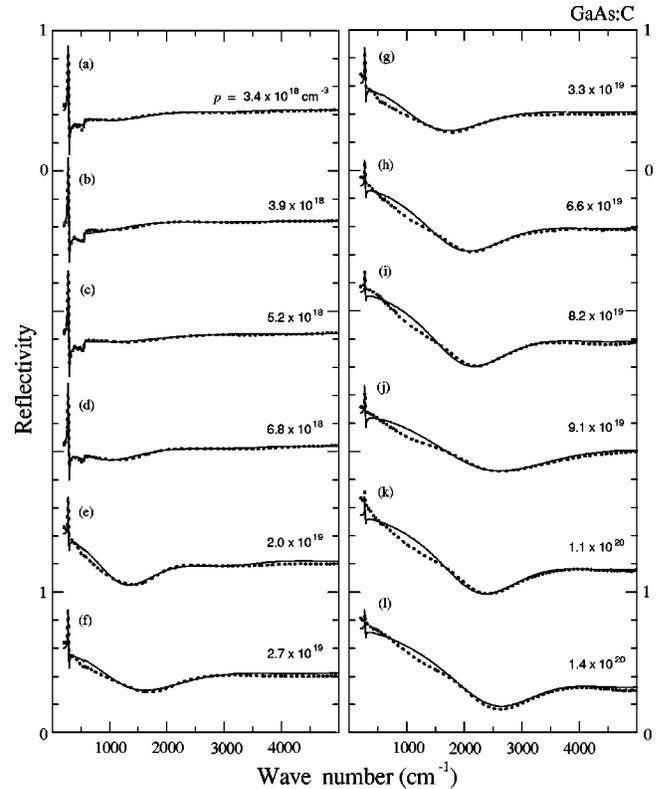
FIG. 1. Reflectivity spectra of 12 p-type GaAs:C MBE films, labeled by their Hall-derived hole concentrations. The solid lines represent the best fits based on Eqs. (1) and (2). The vertical scale is labeled for the top and bottom spectrum in each panel. The other spectra are successively shifted, vertically, by 0.8.

DTGS/POLY detector, and a three-micron-thick mylar beamsplitter were employed for the measurements in the far-infrared (FIR) region (200–700 cm^{-1}). For the mid-infrared (MIR) region (500–5000 cm^{-1}) a DTGS/KBr detector and a KBr beamsplitter were used with the globar source. Spectra were taken at a resolution of 4 cm^{-1}. In order to improve the signal-to-noise ratio, an average over 100 interferogram scans was Fourier-transformed for each spectrum. Signal strength and reflectivity accuracy were better in the MIR region than the FIR, so the FIR reflectivity spectra were rescaled to coincide with the MIR reflectivity spectra in the overlapping region.

III. INFRARED REFLECTIVITY: HOLE PLASMONS IN GaAs:C

Figure 1 presents the experimental reflectivity spectra of twelve MBE p-type GaAs:C films. The thicknesses and transport properties of the films are given in Table I. The spectra exhibit, near 270 cm^{-1}, the one-phonon reststrahlen band. With increasing carbon concentration, a broad reflectivity minimum develops in the 1000–3000 cm^{-1} region. This minimum is a plasmon feature corresponding to the hole plasmon in p-type GaAs. It is much broader than the electron-plasma reflectivity minimum seen in n-type GaAs.[22–24] The phonon band in GaAs:C is also affected by carrier concentration. In samples (a)–(d), with hole concentrations below 10^{19} cm^{-3}, the phonon band is sharp and strong while the plasmon minimum is quite weak. In addi-

TABLE I. Film thickness, Hall-derived hole concentration, and Hall mobility for each of the MBE-grown GaAs:C epitaxial films.

Sample	Thickness d (μm)	p (10^{18} cm^{-3})	μ_{Hall} [cm^2/(V s)]
(a)	0.75	3.4	138
(b)	0.75	3.9	131
(c)	0.50	5.2	127
(d)	0.75	6.8	116
(e)	0.75	20.4	90
(f)	0.50	27.2	87
(g)	0.50	33.1	81
(h)	0.50	65.8	71
(i)	0.50	81.7	68
(j)	0.35	90.6	67
(k)	0.50	105	64
(l)	0.50	136	57

TABLE II. Material parameters of GaAs.

ϵ_∞	High-frequency dielectric constant	10.9[a]
ω_{TO}	TO-phonon frequency	268 cm^{-1} [a]
ω_{LO}	LO-phonon frequency	292 cm^{-1} [a]
Γ	Phonon damping constant	2.5 cm^{-1} [b]
D	Thickness of the GaAs substrate	635 μm

[a]From Ref. 39.
[b]From Ref. 52.

tion, there is a step in reflectivity discernible at about 560 cm^{-1}, the cutoff frequency of the two-phonon absorption.[26] This is a consequence of the substrate's transparency above 560 cm^{-1}, which allows a contribution to the observed reflectivity from light returning from the substrate's back surface.

As p is increased, prominent changes in reflectivity are observed: (i) The one-phonon band decreases and is superimposed on a progressively increasing reflectivity background which comes from the increasing free-carrier contribution to the dielectric function. (ii) The reflectivity minimum becomes more pronounced and moves up to higher frequency. The overall spectral shapes in the one-phonon-band region for our GaAs:C films are similar to those for GaAs:Be films reported in earlier papers,[27,28] and the broad shapes in the reflectivity-minimum region also resemble those for GaAs:C films studied by Wang and Haegel.[15] In addition to the doping effects, the thickness of the GaAs:C film has an influence on the reflectivity. Small film thickness broadens the reflectivity minimum and shifts it up in frequency. This effect is evident in sample (j); because of the small thickness (3500 Å) of this sample, the reflectivity minimum is comparatively broad and occurs at about the same frequency as for the highest doping.

To analyze these data, we have chosen to use the simplest possible form for the dielectric function of the epitaxial GaAs:C film. It is the sum of a single one-phonon lattice-vibrational term (using a classical oscillator model) and a single free-carrier plasma term (using the Drude model),

$$\epsilon = \epsilon_\infty \left(1 + \frac{\omega_{LO}^2 - \omega_{TO}^2}{\omega_{TO}^2 - \omega^2 + i\omega\Gamma} - \frac{\omega_p^2}{\omega^2 - i\omega\gamma} \right). \quad (1)$$

Here ϵ_∞, $\omega_{TO}(\omega_{LO})$, Γ, ω_p, and γ are the high-frequency dielectric constant, the frequency of the transverse (longitudinal) zone-center optic phonon, the phonon damping constant, the plasma frequency, and the plasma damping constant, respectively.

It should be noted that the Drude free-carrier term in Eq. (1) is an approximate one; the exact term, which is derived from the ac conductivity in ac transport theory,[29] requires a statistical average over the free-carrier distribution. The use of the Drude approximation, for our heavily doped samples, will be discussed in Sec. V.

The Drude term in Eq. (1) contains the only two adjustable parameters used in this work, the plasma frequency ω_p and the plasma damping constant γ. The phonon parameters and ϵ_∞ are kept fixed at the known values for undoped GaAs, listed in Table II. We will therefore refer to Eq. (1) as the effective-plasmon dielectric function.

To calculate the reflectivity, we have treated the buffer layer and substrate as one material, using the two-layer model shown in Fig. 2. Since the substrate is semi-insulating, we use, for its dielectric function ϵ_{sub}, the sum of the first two terms in Eq. (1) (omitting the free-carrier term). It is necessary to include the substrate in our analysis because, throughout most of our infrared range, the optical penetration depth exceeds the MBE film thickness.

Solving Maxwell's equations and imposing the boundary conditions at the vacuum/film and film/substrate interfaces, we obtain the reflection coefficient R_a and transmission coefficient T_a for light entering the film from the vacuum side (from the left in Fig. 2), and the corresponding coefficients R_a' and T_a' for light entering the film from the substrate side. The boundary conditions at the film/substrate and substrate/vacuum interfaces lead to very closely spaced interference fringes not seen in the experimental spectra because of the finite resolution. When reflection from the back surface (substrate/vacuum interface) is important because of substrate transparency, these fringes must be averaged out properly. We used the standard technique for achieving this, the intensity-transfer-matrix method.[30,31] In this method, the reflectivity is given by

$$R = R_a + \frac{T_a' R_b T_a e^{-2\alpha_{sub}D}}{1 - R_a' R_b e^{-2\alpha_{sub}D}}, \quad (2)$$

where
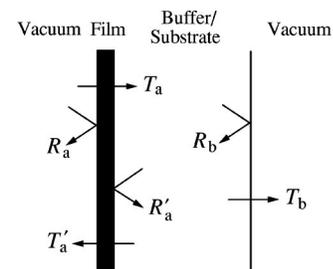
FIG. 2. Schematic diagram of the sample geometry and the notations used for the intensity-transfer-matrix analysis. The solid region represents the MBE GaAs:C film.

TABLE III. The Hall-derived hole concentrations, the carbon concentrations [C] determined from secondary-ion-mass spectroscopy and LVM spectroscopy, and the free-hole parameters of GaAs:C determined from IR measurements.

Sample	p (10^{18} cm^{-3})	[C] (10^{18} cm^{-3})		ω_p (cm^{-1})	γ (cm^{-1})	μ_{IR} [cm^2/(V s)]	μ_{Hall}/μ_{IR}
		SIMS	LVM				
(a)	3.4			520	1420	64	2.2
(b)	3.9		7	360	580	65	2.0
(c)	5.2		10	510	820	71	1.8
(d)	6.8		12	540	940	52	2.2
(e)	20.4		29	930	900	53	1.7
(f)	27.2	26	29	1010	810	52	1.7
(g)	33.1		38	1120	890	48	1.7
(h)	65.8			1510	1070	37	1.9
(i)	81.7			1620	930	39	1.7
(j)	90.6			1780	1190	33	2.0
(k)	105	99		1840	1130	32	2.0
(l)	136	130		2150	1610	24	2.4

$$R_a = \left| \frac{(1-n)(n+n_{sub})+(1+n)(n-n_{sub})e^{-4\pi i n\, d\bar{\nu}}}{(1+n)(n+n_{sub})+(1-n)(n-n_{sub})e^{-4\pi i n\, d\bar{\nu}}} \right|^2, \quad (3)$$

$$R_a' = \left| \frac{(1+n)(n-n_{sub})+(1-n)(n+n_{sub})e^{-4\pi i n\, d\bar{\nu}}}{(1+n)(n+n_{sub})+(1-n)(n-n_{sub})e^{-4\pi i n\, d\bar{\nu}}} \right|^2, \quad (4)$$

$$T_a = \text{Re}(n_{sub})$$
$$\times \left| \frac{4n e^{-2\pi i n d\bar{\nu}}}{(1+n)(n+n_{sub})+(1-n)(n-n_{sub})e^{-4\pi i n\, d\bar{\nu}}} \right|^2, \quad (5)$$

$$T_a' = \frac{1}{\text{Re}(n_{sub})}$$
$$\times \left| \frac{4n n_{sub} e^{-2\pi i n d\bar{\nu}}}{(1+n)(n+n_{sub})+(1-n)(n-n_{sub})e^{-4\pi i n\, d\bar{\nu}}} \right|^2, \quad (6)$$

$$R_b = \left| \frac{n_{sub}-1}{n_{sub}+1} \right|^2, \quad (7)$$

and

$$T_b = \frac{1}{\text{Re}(n_{sub})} \left| \frac{2n_{sub}}{n_{sub}+1} \right|^2. \quad (8)$$

Here n and n_{sub} are the complex refractive indices of the film and substrate, respectively. d and D are the thicknesses of the GaAs:C film and the substrate, respectively. The first term in Eq. (2) is equivalent to the reflectivity of a thin absorbing film on an opaque substrate,[22,27,28,32] and the second term is derived from the sum of a geometric series of multiple re-

flections across the substrate. The quantity given by Eq. (8) will be used in the next section, in connection with our transmittance results.

At frequencies below the two-phonon cutoff near 560 cm^{-1}, $2\alpha_{sub}D \gg 1$ and the substrate can be assumed to be completely opaque because of lattice absorption. Thus the second term in Eq. (2) is negligible at low frequencies, $\bar{\nu} < 560$ cm^{-1}.

The Marquardt method[32-34] was used for performing the nonlinear least-square fitting, with only two parameters, ω_p and γ, varied in searching for the best fit. The GaAs substrate thickness was 635 μm. The GaAs:C film thicknesses were the experimental values of Table I.

The solid lines in Fig. 1 represent the resulting fits. The fits are very reasonable in the high-frequency region containing the plasmon minimum. The best-fit values of ω_p and γ are given in Table III.

Although the presence of a near-surface depletion layer is confirmed by Raman-scattering measurements on our samples,[17] its effect on the infrared reflectivity is negligible because of its small depth (estimated to decrease from 150 to 20 Å, from the lowest to the highest dopings). To check this, we calculated the reflectivity, for each doping, using a three-layer model in which the dielectric function of the topmost layer was set to ϵ_{sub}, as appropriate for the depletion layer.[22] We found that the results for ω_p and γ values hardly differ from those of Table III.

Figure 3 presents a plot of ω_p, the optically determined plasma frequency, against $p^{1/2}$, where p is the hole concentration determined by our Hall-effect measurements. [It is important to note that ω_p is the uncoupled plasma frequency, not the frequency of the actual plasmon-phonon coupled mode L_+. For our higher ω_p values, ω_p and $\omega(L_+)$ scarcely differ.] For a free-hole plasma consisting of a gas of holes having mass m_h^* and concentration p, the plasma frequency is given by

$$\omega_p^2 = \frac{4\pi p e^2}{\epsilon_\infty m_h^*}. \quad (9)$$
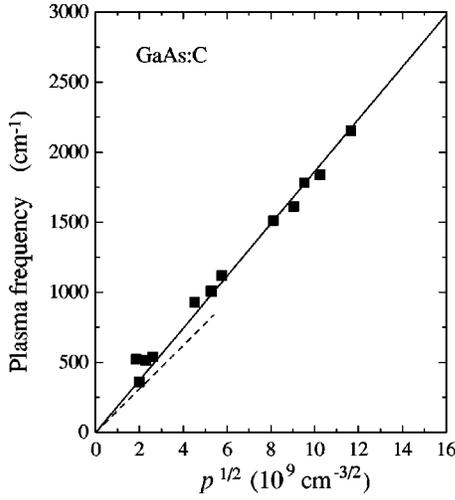
FIG. 3. The dependence of plasma frequency on the square root of Hall-derived hole concentration. The solid squares represent our results. The slope of the solid line corresponds to $m_h^* = 0.24m$. The dashed line represents the calculated plasma frequencies for GaAs:Be (Ref. 28) using $m_h^* = 0.34m$.

As seen in Fig. 3, our results do yield, to within experimental error, a linear relation between ω_p and $p^{1/2}$. This linearity indicates that the concentration dependence of the hole mass is small. We do not find the increase in mass (with increasing p) reported by Wang and Haegel for four GaAs:C samples.[15] The slope of the solid line in Fig. 3 yields an optically derived value, for the average hole effective mass m_h^*, of $0.24m$. The dashed line included in Fig. 3 corresponds to a mass of $0.34m$, which is based on the theoretical expression (from two-band transport theory, Ref. 35) $(m_{lh}^{3/2} + m_{hh}^{3/2})/(m_{lh}^{1/2} + m_{hh}^{1/2})$, where m_{lh} and m_{hh} are the light-hole and heavy-hole masses. This theoretical value was adopted by Fukasawa, Sakai, and Perkowitz (FSP, Ref. 28) in their infrared reflectivity study of p-type GaAs:Be for dopings up to 3×10^{19} cm^{-3}.

Using our optically determined m_h^* [from Eq. (9)] along with the plasma damping constant γ determined for each sample, we have obtained an optical estimate μ_{IR} for the mobility from $\mu_{IR} = e\langle\tau\rangle/m_h^*$. Here $\langle\tau\rangle$ is given by $1/\gamma$, the optical estimate of the free-hole relaxation time. The μ_{IR} values are included in Table III, along with the ratios μ_{Hall}/μ_{IR} comparing the Hall and optical mobilities. Figure 4 shows a plot of μ_{IR} versus μ_{Hall}, and Fig. 5 shows a plot of mobility as a function of hole concentration, comparing our μ_{Hall} and μ_{IR} mobility results to μ_{Hall} for GaAs:C reported in earlier studies.[3–5,12]

Although our m_h^* value is different from the theoretical value adopted by FSP (Ref. 28) in their work on GaAs:Be, the mobility results for p-type GaAs:C shown in Fig. 4 agree well with their results for p-type GaAs:Be. The slope of the fitted straight line in Fig. 4 corresponds to a μ_{Hall}/μ_{IR} ratio of 1.9. The disagreement between μ_{Hall} and μ_{IR} is discussed in Sec. V.

IV. FREE-HOLE AND INTERVALENCE-BAND ABSORPTION

Figure 6 presents our absorbance spectra for five MBE GaAs:C films of 0.5-μm thickness. The experimental absor-
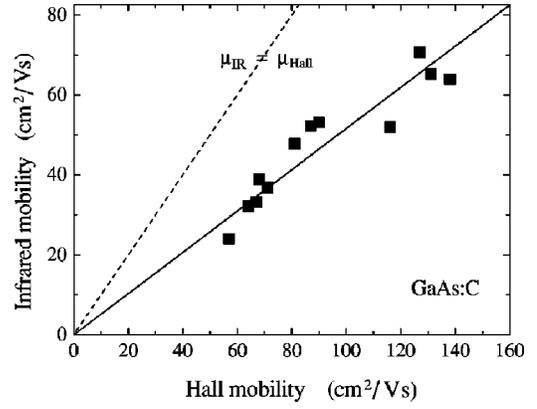
FIG. 4. The Hall mobility μ_{Hall} plotted against the infrared mobility μ_{IR}. The ratio μ_{Hall}/μ_{IR} varies from 1.7 to 2.4 over the 12 samples (Table III). The solid line represents the average ratio of 1.9.

bance A, shown by the points in Fig. 6, was determined from the measured reflectivity R and transmittance T by using $A = 1 - R - T$.[31] A broad absorbance band develops in the same region (1000–3000 cm^{-1}) as the reflectivity minima of Fig. 1, and it shifts to higher frequency as p is increased.

The solid lines in Fig. 6 are calculated curves based on the effective-plasmon dielectric function of Eq. (1), using the ω_p and γ values of Table III (the same plasma parameters as those used to fit the reflectivity results of Fig. 1). The theoretical curves of Fig. 6, like those of Fig. 1, include the phonon contribution contained in Eq. (1), with the phonon parameters of Table II. The phonon contribution has very little effect for $\bar{\nu}$ above 1000 cm^{-1}. The curves of Fig. 6 are obtained from $1 - R - T$, where R and T are now the calculated reflectivity and transmittance. R corresponds to Eqs. (1)–(7) and the solid lines in Fig. 1. T is calculated using the intensity-transfer matrix method described in Sec. III:

$$T = \frac{T_a T_b e^{-\alpha_{sub}D}}{1 - R_a' R_b e^{-2\alpha_{sub}D}}. \qquad (10)$$

All of the quantities on the right side of Eq. (10) are defined in Sec. III.
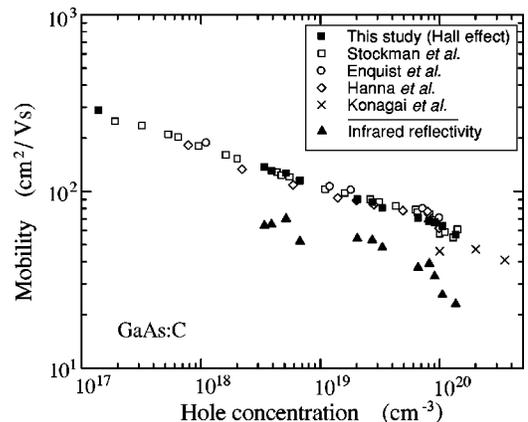
FIG. 5. Mobility versus hole concentration for GaAs:C. The solid squares (dc) and solid triangles (infrared) are our results, the other Hall mobilities are from Refs. 3–5 and 12.
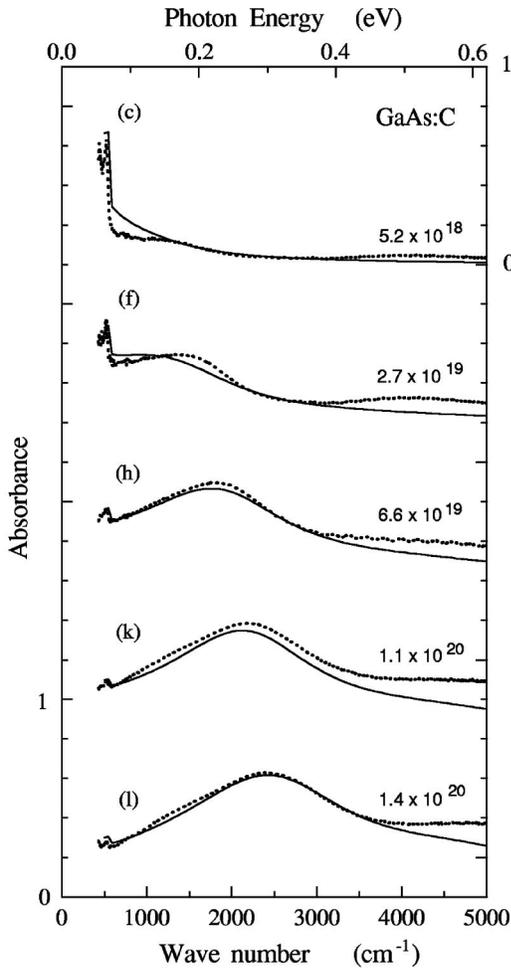
FIG. 6. Absorbance spectra of five p-type GaAs:C MBE films of thickness 0.5 μm, labeled by their Hall-derived hole concentrations. The solid lines are the calculated absorbances based on the effective-plasmon dielectric function of Eq. (1), using the ω_p and γ values of Table III. The vertical scale is labeled for the top and bottom spectrum; the other spectra are successively shifted, vertically, by 0.8. As in Fig. 1, the step seen near 600 cm^{-1} is the substrate's two-phonon cutoff.

The effective-plasmon curves of Fig. 6 give a fairly good account of the broad absorbance maxima exhibited by the GaAs:C films. The experimental spectra also exhibit an additional absorbance contribution at high photon energy.

Absorbance is thickness dependent, and we want a measure of absorption that depends only on the film material, namely, the optical absorption coefficient $\alpha(\bar{\nu})$. The layer geometry introduces a complexity which prohibits a reliable direct path to $\alpha(\bar{\nu})$ from the experimental $A(\bar{\nu})$ measurements. However, it is straightforward to calculate $\alpha(\bar{\nu})$ curves that correspond to the theoretical $A(\bar{\nu})$ curves of Fig. 6, since these are derived from the dielectric function of Eq. (1) with the phonon and plasmon parameters of Tables II and III. Figure 6 shows that the effective-plasmon $A(\bar{\nu})$ curves give a reasonably good representation of the main feature exhibited by the experimental absorbance spectra, the broad maximum in the 1000–3000 cm^{-1} (0.1–0.4 eV) region. The corresponding effective-plasmon absorption-coefficient curves are displayed in the upper portion of Fig. 7, labeled
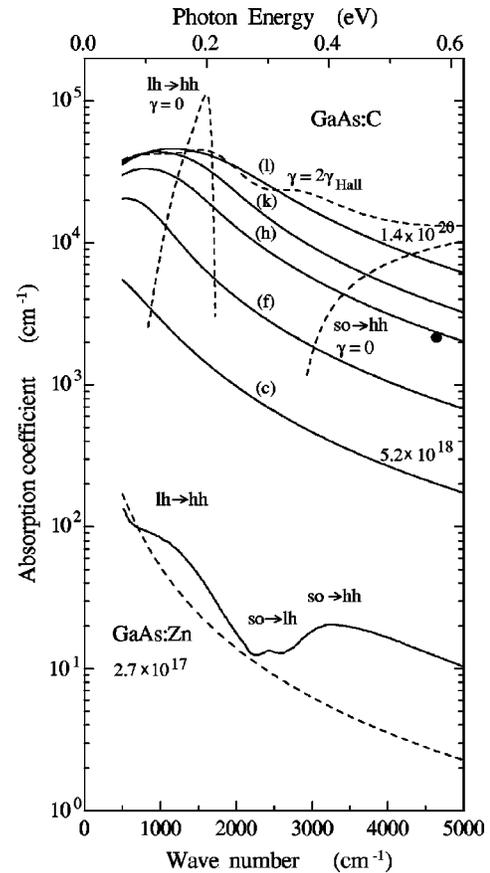
FIG. 7. The effective-plasmon absorption-coefficient spectra for the five GaAs:C films of Fig. 6. Also shown is Braunstein's famous $\alpha(\bar{\nu})$ spectrum (Refs. 36 and 37) for GaAs:Zn. The dashed lines are theoretical curves described in the text. The solid dot, also described in the text, is an estimate for $p = 6 \times 10^{19}$ cm^{-3} based on scaling the GaAs:Zn so→hh maximum from the known experimental behavior of p-Ge.

by the samples whose $\alpha(\bar{\nu})$ they represent. At high doping, these curves develop a broad low-frequency maximum. This is a consequence of the large effective-plasmon damping constant γ.

Also included in Fig. 7 is Braunstein's classic $\alpha(\bar{\nu})$ spectrum[36,37] for GaAs:Zn at $p = 2.7 \times 10^{17}$ cm^{-3}, which was successfully explained by Kane[37,38] in terms of direct transitions among the heavy-hole (hh), light-hole (lh), and split-off (so) valence bands near $k=0$. At $k=0$, the hh and lh bands meet, and the so band is lower by the spin-orbit splitting Δ. (At room temperature, Δ is 0.34 eV for GaAs.[39]) Away from $k=0$, the lh→hh separation approaches $(2/3)\Delta$.[38] Intervalence-band (IVB) transitions among the three bands are both Raman and infrared allowed.[40] Though the infrared activity might have been expected to be weak, because all three bands are derived from p-like states,[21] they are obviously strong enough to be observed. In Raman scattering, pronounced IVB bands have been observed in heavily doped p-type GaAs.[17,21] The electronic IVB transitions responsible for the structure in the GaAs:Zn spectrum are indicated on Fig. 7. The lh→hh and so→hh absorption peaks are much stronger than the so→lh peak, since it is the hh band which holds most of the holes. The photon-energy scale for these features is set by the spin-orbit splitting; the low-energy cut-

off of the so→hh absorption process is at $h\nu=\Delta$, the high-energy cutoff of the lh→hh absorption process is at $(2/3)\Delta$.[37,38]

In this infrared region, intervalence-band direct transitions provide a parallel optical-absorption pathway in competition with free-carrier intraband indirect transitions. The dashed curve near the bottom of Fig. 7 is a free-carrier $\alpha(h\nu)$ curve for the hole concentration of the GaAs:Zn sample, using an infrared hole mobility taken to be half the Hall mobility at this concentration. The infrared mobility will be discussed in the following section.

Our $\alpha(h\nu)$ curves for samples (c), (f), (h), (k), (l) do not show the detailed structure exhibited by the relatively lightly-doped GaAs:Zn sample. A simple scaling (upward shift), of the GaAs:Zn spectrum in Fig. 7, is incorrect because the k-space hole occupation of the hh and lh valence bands increases with doping, as does the ionized impurity scattering. The only semiconductor for which an experimental study[41] has been made of the IVB absorption, for hole concentrations spanning a very wide range, is germanium, whose valence-band structure is similar to that of GaAs. In that study, whose authors emphasize the high-doping importance of ionized-impurity scattering, the so→hh $\alpha(h\nu)$ peak in p-Ge could be followed up to $p=6\times10^{19}$ cm^{-3}, at which doping it had upshifted and broadened nearly beyond recognition, with a barely discernible maximum.[41] No maximum remained at 1.5×10^{20} cm^{-3}. We have used those data for the p-dependence of the so→hh maximum in p-Ge to rescale, both in strength and position, the so→hh maximum in GaAs:Zn to $p=6\times10^{19}$ cm^{-3}. The result is represented by the solid dot in Fig. 7. This point lies close to the curve for sample (h), for which $p=6.6\times10^{19}$ cm^{-3}.

Recently, combining Kane's $\mathbf{k}\cdot\mathbf{p}$ theory[38] with current knowledge of GaAs valence-band parameters (m_{hh}, m_{lh}, Δ), Huberman et $al.$[42] calculated $\alpha(h\nu)$ for degenerate p-GaAs at 0 K. Their work included free-carrier absorption and IVB lh→hh absorption in an isotropic-band approximation. Using Huberman et $al.$'s isotropic-approximation expressions, and additionally including the IVB so→lh and IVB so→hh absorptions via Kane's theory, we have calculated $\alpha(h\nu)$ at 300 K (using Fermi statistics) for $p=1.4\times10^{20}$ cm^{-3}. Our calculation includes a lifetime broadening γ for the interband transitions. We use $\gamma=2\gamma_{\text{Hall}}$, in line with our measured $\mu_{\text{Hall}}/\mu_{\text{IR}}$ ratio and similar to the $\gamma=3\gamma_{\text{Hall}}$ choice used by Huberman et $al.$ to obtain results resembling their own data for GaAs:Be. Our calculated $\alpha(h\nu)$ is the gently varying dashed curve at the top of Fig. 7. There are two shallow maxima in the theoretical curve which occur near the broad effective-plasmon maximum for sample (l). The maximum at about 0.1 eV comes from the free-carrier absorption, and the maximum at about 0.2 eV comes from the lh→hh IVB absorption. Also included in Fig. 7 are calculations based on Kane's theory[38] for the lh→hh and so→hh transitions, using Fermi statistics. These calculations omit lifetime broadening, giving too-sharp features at room temperature.

The theoretical $\alpha(h\nu)$ curve at the top of Fig. 7 closely overlaps the effective-plasmon curve up to about 0.35 eV. Above this photon energy, the effective-plasmon curve is lower. In Fig. 6, it can also be seen that, above about 0.4 eV, the effective-plasmon curve falls below the experimental absorbance. We attribute this above-0.4-eV shortfall to so
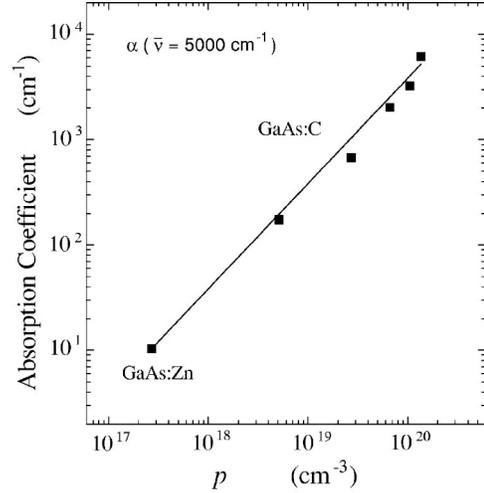
FIG. 8. The p dependence of the absorption coefficient at $\bar{\nu}=5000$ cm^{-1} ($h\nu=0.62$ eV).

→hh transitions, which the effective-plasmon model is less effective in mimicking than the low-energy lh→hh transitions.

From the results and comparisons contained in Fig. 7, we conclude the following. Our experimentally determined effective-plasmon curves, which give a good description of the experimental observations for both reflectivity and transmittance, arise from a combination of two comparable-strength absorption processes: free-carrier intraband transitions and intervalence-band transitions. Both processes should scale roughly with p (though the spectral shapes change appreciably for the IVB features, which smear out and merge at high doping[41]). In Fig. 8, we plot the p dependence of the value of the absorption coefficient at $\bar{\nu}=5000$ cm^{-1} ($h\nu=0.62$ eV), where the IVB absorption (arising, here, from so→hh transitions) is flat and featureless. The free-carrier absorption in this region is closely proportional to (p/ν^2), the λ^2 law. The observed effective-plasmon alphas for the high-p GaAs:C samples of Figs. 6 and 7 are shown, as is the low-p GaAs:Zn alpha of Braunstein.[36,37] The same $\alpha\propto p$ line describes both sets of infrared data; the α/p cross section is 4×10^{-17} cm^2. The straight-line match of Fig. 8 may be fortuitous, because Figs. 6 and 7 indicate that the effective-plasmon model underestimates α in the so→hh region. However, the dominant lh→hh IVB absorption band is evidently efficiently included in the effective-plasmon α.

Experimental infrared measurements on p-GaAs (or any p-type III-V semiconductor, since all have similar band structures near the valence-band edge) will thus inevitably admix free-carrier and intervalence-band contributions. We have used a free-carrier effective-plasmon form for the dielectric function, with only two adjustable (best-fit) parameters, and have found it to yield a good phenomenological description of the measured infrared reflectivity and absorbance spectra. It is evident that the effective-plasmon parameters include the influence of the intervalence-band contribution.

V. HOLE MOBILITY: INFRARED VERSUS HALL

The two estimates of average hole drift mobility, μ_{IR} and μ_{Hall}, differ by a factor of 1.9. Which is the better estimate

for the actual hole drift mobility in GaAs:C?

In their work on GaAs:Be, Fukasawa, Sakai, and Perkowitz,[28] who obtained a similar result (2.0) for the $\mu_{\text{Hall}}/\mu_{\text{IR}}$ ratio, presented a plausible argument for interpreting μ_{IR} as the hole drift mobility. This is based on the Hall factor, a dimensionless quantity of order unity which enters into the determination of μ_{Hall}. The measured quantities in Hall-effect experiments are the resistivity $\rho = 1/(p\,e\,\mu)$ and the Hall coefficient R_{H}. The mobility μ_{Hall} and carrier concentration p_{Hall} are then determined from

$$\mu_{\text{Hall}} = \frac{R_{\text{H}}}{\rho} \qquad (11)$$

and

$$p_{\text{Hall}} = \frac{1}{R_{\text{H}}\,e}. \qquad (12)$$

We have now added the subscript 'Hall' to the hole concentration p_{Hall} determined by Hall measurements. The p values used throughout this paper (Tables I and II) are p_{Hall} values.

It has long been known that a numerical factor, now called the Hall factor r_{Hall}, intervenes in the relation connecting R_{H} and the (actual) carrier concentration p,[43]

$$R_{\text{H}} = \frac{r_{\text{Hall}}}{p\,e}. \qquad (13)$$

Here the Hall factor r_{Hall} is given by[29,44]

$$r_{\text{Hall}} = \frac{\langle \tau^2/(m^*)^2 \rangle}{\langle \tau/m^* \rangle^2}, \qquad (14)$$

where τ is the energy-dependent Boltzmann-equation relaxation time and $\langle\ \rangle$ denotes the Fermi-Dirac statistical weighted average over the free-carrier distribution. The Hall factor reduces to $r_{\text{Hall}} = \langle \tau^2 \rangle / \langle \tau \rangle^2$ for free carriers of a single type.[43,45,46] The relations between the Hall-determined quantities (μ_{Hall} and p_{Hall}) and the actual quantities (μ and p) are

$$\mu = \frac{1}{r_{\text{Hall}}} \mu_{\text{Hall}} \qquad (15)$$

and

$$p = r_{\text{Hall}}\, p_{\text{Hall}}. \qquad (16)$$

The Hall factor r_{Hall} is routinely ignored in Hall-effect determinations of mobility and carrier concentration, in which the measured μ_{Hall} and p_{Hall} are taken to be synonymous with μ and p. This is equivalent to assuming that $r_{\text{Hall}} = 1$. [From Eq. (14), it may be expected that r_{Hall} is slightly larger than 1.0.] To quote Ziman,[43] ''This correction is not usually important compared with the other errors inherent in the calculation.'' Assuming that $r_{\text{Hall}} = 1$, as we have done to this point, is standard operating procedure in Hall measurements.

Fukasawa, Sakai, and Perkowitz interpret the disparity between μ_{Hall} and μ_{IR} as arising entirely from the Hall factor.[28] This interpretation identifies μ_{IR} as the true drift mobility μ. From Eq. (15), the ratio then corresponds to r_{Hall}, so that $r_{\text{Hall}} = 2.0$. FSP point out that reported theoretical calculations[44,48] of r_{Hall} for p-type GaAs give a range of values that do extend as high as 2. Thus their interpretation of $\mu_{\text{Hall}}/\mu_{\text{IR}}$ as r_{Hall} (and their identification of μ_{IR} as μ) appears plausible.

The problem is that if $r_{\text{Hall}} = 2.0$ and the measured Hall mobility overestimates [from Eq. (15)] the true drift mobility by a factor of 2, it then follows [from Eq. (16)] that the Hall-derived hole concentration underestimates the true hole concentration by a factor of 2, so that $p = 2p_{\text{Hall}}$. In our own work here on GaAs:C, we have results that contradict this possibility. For several of our samples, we have experimental estimates of the dopant concentration [C] obtained by secondary ion mass spectroscopy (SIMS) and localized vibrational mode spectroscopy (LVM).[25] These estimates are contained in Table III. To within experimental error (estimated to be $\pm 20\%$ for [C]), these results are consistent with approximate equality of p and [C], i.e., close to full activation of C_{As} donors. This is what is expected, and it agrees with a substantial body of reported work[1,3,8,13,47] for GaAs:C. But if our (Hall-derived) p values were too low by a factor of 2 (as required by $r_{\text{Hall}} = 2.0$), this would correspond to a hole concentration that is twice the carbon concentration, which is highly implausible. We therefore conclude that r_{Hall} cannot be 2.0, but is instead much closer to 1.0. Support for this comes from recent work[49] which finds that r_{Hall} is close to 1.0 for p larger than 3×10^{18} cm^{-3} (our concentration range) in p-GaAs. We conclude that the Hall-derived p values given in Tables I and III are reasonable estimates of the actual hole concentrations, and that the Hall mobilities in Table I are reasonable estimates of the dc drift mobility in these samples.

It should be noted that statistical subtleties, similar to those which introduce r_{Hall} in Hall-effect experiments, also plague the identification of μ_{IR} (as the true drift mobility) in infrared experiments. In the IR analysis, the ac conductivity $\sigma(\omega)$ is taken to have the simple form

$$\sigma(\omega) = \frac{p\,e^2}{m^*} \frac{\langle \tau \rangle}{1 + i\omega\langle \tau \rangle}, \qquad (17)$$

instead of the more rigorous form[29,50]

$$\sigma(\omega) = \frac{p\,e^2}{m^*} \left\langle \frac{\tau}{1 + i\omega\tau} \right\rangle. \qquad (18)$$

This approximation avoids the requirement of averaging, at each IR frequency ω, over the carrier-energy distribution. Lyden[51] carried out a detailed analysis of the effect of this standard IR-analysis approximation, for different scattering mechanisms and different degrees of degeneracy η, where $\eta = (E_v - E_F)/kT$ for p-type semiconductors. For ionized-impurity scattering [which is the dominant room-temperature scattering mechanism in heavily-doped GaAs:C (Refs. 44 and 49)], his analysis shows that the standard IR-analysis approximation can yield a best-fit τ that differs from the true value of $\langle \tau \rangle$ by nearly a factor of 2 for low (nondegenerate) doping. But with increased doping, the error decreases, and Lyden's work shows the error to be entirely negligible for highly degenerate samples ($\eta > 4$). Thus the statistical complication in the analysis for τ_{IR} (and μ_{IR}) disappears in the degenerate limit.

Among our 12 GaAs:C MBE films, the five highest dopings [samples (h)–(l)] are highly degenerate (room-temperature η values: 4.2, 4.9, 5.2, 5.8, 6.9). For these samples, the approximation involved in the use of the standard infrared analysis is a good one. In addition, for these samples we have carried out calculations of the proper statistical average at a set of closely spaced frequencies, using $\tau(E)$ proportional to $E^{3/2}$ (where E is carrier kinetic energy) as appropriate for ionized-impurity scattering.[51] The best fits from this method closely reproduce the Drude fits, with insignificant improvement from using the more rigorous procedure. And the results for ω_p and γ are essentially unchanged from the Drude-fit values of Table III.

We conclude that this result for heavily-doped p-type GaAs, $\mu_{IR}/\mu_{Hall} \approx 1/2$, is real. The dichotomy between the two mobilities is not an artifact of the statistical subtleties involved in either the infrared or the Hall analyses. Our μ_{Hall} and μ_{IR} results represent good estimates, for p-type GaAs at these dopings, of the mobilities at dc and infrared frequencies. Thus the hole relaxation time at infrared frequencies, $\langle\tau\rangle_{IR}$, is significantly smaller than the relaxation time in dc fields. This stands in contrast to the situation in n-type GaAs, for which μ_{IR} and μ_{Hall} do not disagree.[22,23]

The standard experimental method used for determining $\langle\tau\rangle_{IR}$ is the one we have used in Sec. III; $\langle\tau\rangle_{IR} = \gamma^{-1}$, where γ is obtained from an effective-plasmon fit to the infrared reflectivity.[22,23,28] But as we have shown in Sec. IV, for p-type GaAs the infrared optical properties include an important contribution from intervalence-band transitions. The effective-plasmon model is reasonably successful in describing or incorporating the main IVB component (the lh→hh band) in the form of a broad band associated with the large γ called for by the fit. The large γ is thus a consequence of the intervalence-band optical absorption in the infrared. Hence $\langle\tau\rangle_{IR} = \gamma^{-1}$ is small, hence μ_{IR} is small. This resolves the dilemma of the μ_{IR}/μ_{Hall} ''discrepancy'' in p-type GaAs. This infrared/dc mobility dichotomy should also be found in other p-type semiconductors with closely spaced valence bands and significant intervalence-band infrared absorption.

VI. CONCLUSIONS

Heavily-doped p-type GaAs:C films were grown by molecular-beam epitaxy, with Hall-derived hole concentrations p_{Hall} up to 1.4×10^{20} cm^{-3}. SIMS and LVM measurements show that p_{Hall} is close to the carbon concentration [C], in agreement with previous work and consistent with the use of p_{Hall} as a good measure of the actual hole concentration p. Thus the Hall factor r_{Hall}, which enters in Eqs. (15)

and (16), is close to unity, so that the Hall mobility μ_{Hall} (results shown as the solid squares in Fig. 5) also provides a good estimate of the dc mobility.

Infrared reflectivity measurements were carried out on the GaAs:C films over the spectral range from 200 to 5000 cm^{-1}, and transmittance measurements were carried out from 500 to 5000 cm^{-1}. With increasing doping, the low-frequency reflectivity increases while a reflectivity minimum develops at high frequency which becomes more pronounced and shifts to higher frequency as p increases. An effective-plasmon dielectric function with only two free parameters (ω_p and γ), used as input to an intensity-transfer-matrix-method optical calculation appropriate to our film/substrate geometry, gives a good description of the reflectivity spectra of Fig. 1. The same effective-plasmon dielectric functions also give a good account of the observed absorbance spectra (Fig. 6).

The comparisons contained in Fig. 7 reveal that, in addition to free-carrier (hole) absorption, intervalence-band direct transitions contribute significantly to the observed infrared absorption. This is indicated by a rescaling (via p-Ge high-p data) of Braunstein's low-p GaAs:Zn spectra and by a $\mathbf{k}\cdot\mathbf{p}$ calculation extending Kane's theory to our high dopings. The comparisons show that the effective-plasmon model simulates or incorporates the contribution of the main (lh→hh) intervalence-band absorption band by means of a large γ, which translates into a small optical mobility μ_{IR}.

The measured infrared mobility in GaAs:C is about half the dc mobility (Figs. 4 and 5). For our five highest dopings, our samples are well within the degenerate regime, and for this situation the statistical approximations involved in the use of the Drude infrared analysis are justified. A similar statement applies to the dc mobility, since the Hall factor is close to unity in the ionized-impurity-dominated high-doping regime. Thus the observed dichotomy between the dc and infrared mobilities is real, not a statistical-averaging artifact. The explanation of the small infrared mobility resides in the influence of intervalence-band absorption on the effective-plasmon damping that operationally determines μ_{IR}. For n-GaAs, which lacks infrared interband absorption, the dc and IR mobilities do not differ.

---

*Present address: Lucent Technologies, Breinigsville, PA 18051.

[1] B. P. Yan, J. S. Luo, and Q. L. Zhang, Acta Phys. Sin. **4**, 531 (1995).

[2] K. Mochizuki and T. Nakamura, Appl. Phys. Lett. **65**, 2066 (1994).

[3] S. A. Stockman, G. E. Hofler, J. N. Baillargeon, K. C. Hsieh, K. Y. Cheng, and G. E. Stillman, J. Appl. Phys. **72**, 981 (1992).

[4] P. M. Enquist, Appl. Phys. Lett. **57**, 2348 (1990).

[5] M. C. Hanna, Z. H. Lu, and A. Majerfeld, Appl. Phys. Lett. **58**, 164 (1991).

[6] S. Tanaka, M. Ito, M. Ikeda, and T. Kikuta, J. Cryst. Growth **124**, 812 (1992).

[7] H. Wu and Z. Li, J. Cryst. Growth **167**, 429 (1996).

[8] T. B. Joyce, S. P. Westwater, P. J. Goodhew, and R. E. Pritchard, J. Cryst. Growth **164**, 371 (1996).

[9] K. Saito, E. Tokumitsu, T. Akatsuka, M. Miyauchi, T. Yamada, M. Konagai, and K. Takahashi, J. Appl. Phys. **64**, 3975 (1988).

[10] K. Zhang, W. Y. Hwang, D. L. Miller, and L. W. Kapitan, Appl. Phys. Lett. **63**, 2399 (1993).

[11] K. Ouchi, T. Mishima, K. Mochizuki, T. Oka, and T. Tanoue,

Jpn. J. Appl. Phys., Part 1, **36**, 1866 (1997).

[12] M. Konagai, T. Yamada, T. Akatsuka, K. Saito, E. Tokumitsu, and K. Takehashi, J. Cryst. Growth **98**, 167 (1989).

[13] I. Fujimoto, S. Nishine, T. Yamada, M. Konagai, and K. Takahashi, Jpn. J. Appl. Phys., Part 2, **31**, L296 (1992); M. Shirahama, K. Nagao, E. Tokumitsu, M. Konagai, and K. Takahashi, Jpn. J. Appl. Phys., Part 1, **32**, 5473 (1993).

[14] B. P. Yan, J. S. Luo, and Q. L. Zhang, J. Appl. Phys. **77**, 4822 (1995).

[15] L. Wang and N. M. Haegel, in *Advanced III-V Compound Semiconductor Growth, Processing and Devices*, edited by S. J. Pearton, D. K. Sadana, and J. M. Zavada, Mater. Res. Soc. Symp. Proc. Proceedings No. **240** (Materials Research Society, Pittsburgh, 1992), p. 87.

[16] M. Seon, M. Holtz, W. M. Duncan, and T. S. Kim, J. Appl. Phys. **85**, 7224 (1999).

[17] R. Zallen, W. Songprakob, S. Vijarnwannaluk, M. L. Hsieh, R. A. Stradling, W. K. Liu, and K. L. Bacher, Bull. Am. Phys. Soc. **44**, 1679 (1999). Room-temperature photoluminescence and Raman-scattering measurements were carried out on our GaAs:C films in near back-scattering geometry. The small penetration depth of the laser lines used limited the observed scattering processes to the MBE GaAs:C layer. Raman scattering by the lower-frequency coupled-LO-phonon-plasmon mode (the phononlike L_- mode) was observed, but no plasmonlike L_+ mode was seen. Intervalence-band Raman scattering was observed, as was photoluminescence involving the split-off valence band. The unscreened LO-phonon line was present in the Raman spectrum; it arises from the presence of the depletion layer beneath the front surface of the film. With increasing doping, the depth of the depletion layer decreases. The Raman measurements monitored the depletion-layer depth from the strength of the LO line.

[18] D. Olego and M. Cardona, Phys. Rev. B **24**, 7217 (1981).

[19] R. Fukasawa and S. Perkowitz, Phys. Rev. B **50**, 14 119 (1994).

[20] R. A. Munoz-Hernandez, S. Jiminez-Sandoval, G. Torres-Delgado, C. Roch, X. K. Chen, and J. C. Irwin, J. Appl. Phys. **80**, 2388 (1996).

[21] D. Olego, M. Cardona, and U. Rossler, Phys. Rev. B **22**, 1905 (1980).

[22] R. T. Holm, J. W. Gibson, and E. D. Palik, J. Appl. Phys. **48**, 212 (1977).

[23] S. Perkowitz and J. Breecher, Infrared Phys. **13**, 321 (1973).

[24] H. R. Chandrasekhar and A. K. Ramdas, Phys. Rev. B **21**, 1511 (1980).

[25] L. Sargent and J. S. Blakemore, Appl. Phys. Lett. **54**, 1013 (1989); S. Vijarnwannaluk, W. Songprakob, R. Zallen, W. K. Liu, and K. L. Bacher, Bull. Am. Phys. Soc. **44**, 1678 (1999).

[26] W. Cochran, S. J. Fray, F. A. Johnson, J. E. Quarrington, and N. Williams, J. Appl. Phys. **32**, 2102 (1961).

[27] R. Fukasawa, M. Wakaki, and K. Ohta, Jpn. J. Appl. Phys., Part 1, **31**, 2138 (1992).

[28] R. Fukasawa, K. Sakai, and S. Perkowitz, Jpn. J. Appl. Phys., Part 1 **36**, 5543 (1997).

[29] E. Conwell, in *Handbook on Semiconductors*, edited by W. Paul (North-Holland Publishing, New York, 1982), Vol. 1, pp. 530–539.

[30] T. W. Noh, P. H. Song, Sung Ik Lee, D. C. Harris, J. R. Gaines, and J. C. Garland, Phys. Rev. B **46**, 4212 (1992).

[31] R. F. Potter, in *Handbook of Optical Constants of Solids*, edited by E. D. Palik (Academic Press, Olando, 1985), p. 22.

[32] Y. B. Li, R. A. Stradling, T. Knight, J. R. Birch, R. H. Thomas, C. C. Phillips, and I. T. Ferguson, Semicond. Sci. Technol. **8**, 101 (1993).

[33] D. W. Marquardt, J. Soc. Ind. Appl. Math. **11**, 431 (1963).

[34] P. R. Bevington and D. K. Robinson, *Data Reduction and Error Analysis for the Physical Sciences* (McGraw-Hill, Singapore, 1992), pp. 161–164.

[35] J. D. Wiley and M. DiDomenico, Phys. Rev. B **2**, 427 (1970); J. D. Wiley, in *Semiconductors and Semimetals*, edited by R. K. Willardson and A. C. Beer (Academic Press, New York, 1975), Vol. 10, p. 91.

[36] R. Braunstein, J. Phys. Chem. Solids **8**, 280 (1959).

[37] R. Braunstein and E. O. Kane, J. Phys. Chem. Solids **23**, 1423 (1962).

[38] E. O. Kane, J. Phys. Chem. Solids **1**, 82 (1956).

[39] J. S. Blakemore, J. Appl. Phys. **53**, R123 (1982).

[40] G. Dresselhaus, Phys. Rev. **100**, 580 (1955); R. H. Parmenter, *ibid.* **100**, 573 (1995).

[41] R. Newman and W. W. Tyler, Phys. Rev. **105**, 885 (1957).

[42] M. L. Huberman, A. Ksendov, A. Larsson, R. Terhune, and J. Maserjian, Phys. Rev. B **44**, 1128 (1991).

[43] J. M. Ziman, *Electrons and Phonons* (Oxford University Press, London, 1960), p. 490.

[44] B. W. Kim and A. Majerfeld, J. Appl. Phys. **79**, 1939 (1996).

[45] K. Seeger, *Semiconductor Physics* (Springer-Verlag, Berlin, 1997), p. 59.

[46] P. Y. Yu and M. Cardona, *Fundamentals of Semiconductors* (Springer-Verlag, Berlin, 1996), p. 227.

[47] T. J. deLyon, J. M. Woodall, M. S. Goorsky, and P. D. Kirchner, Appl. Phys. Lett. **56**, 1040 (1990).

[48] H. J. Lee and D. C. Look, J. Appl. Phys. **54**, 4446 (1983).

[49] M. Wenzel, G. Irmer, J. Monecke, and W. Siegel, J. Appl. Phys. **81**, 7810 (1997); Semicond. Sci. Technol. **13**, 505 (1998). Figure 6 of the 1997 paper and Fig. 4(a) of the 1998 paper show that the Hall mobility and the drift mobility coincide at high doping, where ionized impurity scattering dominates.

[50] P. N. Butcher, in *Handbook on Semiconductors*, edited by W. Paul (North-Holland Publishing, New York, 1982), p. 702.

[51] H. A. Lyden, Phys. Rev. **134**, A1106 (1964).

[52] O. K. Kim and W. G. Spitzer, J. Appl. Phys. **50**, 4362 (1979).